42nd AIAA/ASME/SAE/ASEE Joint Propulsion Conference & Exhibit
9 - 12 July 2006, Sacramento, California

AIAA 2006-4831

Kinetic Effects in Hall Thruster Discharge

I. D. Kaganovich[1] and Y. Raitses [2]
Plasma Physics Laboratory, Princeton University, Princeton, NJ, 08543, USA

and

D. Sydorenko[3] and A. Smolyakov[4]
University of Saskatchewan, Saskatoon, SK, S7H3E6, Canada

Recent analytical studies and particle-in-cell simulations suggested that the electron velocity distribution function in a Hall thruster plasma is non-Maxwellian and anisotropic.[1,2] The electron average kinetic energy in the direction parallel to walls is several times larger than the electron average kinetic energy in direction normal to the walls. Electrons are stratified into several groups depending on their origin (e.g., plasma discharge or thruster channel walls) and confinement (e.g., lost on the walls or trapped in the plasma). Practical analytical formulas are derived for wall fluxes, secondary electron fluxes, plasma parameters, and conductivity. The calculations based on analytical formulas agree well with the results of numerical simulations. The self-consistent analysis demonstrates that elastic electron scattering on collisions with atoms and ions plays a key role in formation of the electron energy distribution function and plasma-wall interaction. The fluxes of electrons from the plasma bulk are shown to be proportional to the rate of scattering to loss cone, thus collision frequency determines the wall potential and secondary electron fluxes. Secondary electron emission from the walls is shown to enhance the electron conductivity across the magnetic field, while having almost no effect on insulating properties of the near-wall sheaths. Such a self-consistent decoupling between secondary electron emission effects on electron energy losses and electron crossed-field transport is currently not captured by the existing fluid and hybrid models of the Hall thrusters.

Nomenclature

x	= coordinate normal to the walls, along the applied magnetic field
z	= coordinate parallel to the walls, along the applied electric field
t	= time
$v_{x,y,z}$	= electron velocity components
w	= electron kinetic energy
$w_{x,y,z}$	= kinetic energy of electron motion in the x, y, and z direction respectively
m	= electron mass
M	= ion mass
e	= elementary charge
H	= width of the plasma slab
$E_{x,z}$	= components of the electric field intensity (the self-consistent field is normal to the wall)
B_x	= induction of the applied magnetic field
Φ	= electrostatic potential relative to the dielectric wall at x = H
n_a	= neutral gas density
n_e	= electron density

[1]Research physicist, Princeton Plasma Physics Laboratory, ikaganov@pppl.gov
[2]Research physicist, Princeton Plasma Physics Laboratory, yraitses@pppl.gov, AIAA member.
[3]Graduate student, Department of Physics and Engineering Physics, dms169@mail.usask.ca
[4]Professor, Department of Physics and Engineering Physics, andrei.smolyakov@usask.ca

ν_{turb} = frequency of "turbulent" collisions
ν_{en} = frequency of electron-neutral collisions
λ_c = electron mean free path between two collisions
μ_c = collisional electron mobility across the magnetic field
r_L = electron Larmor radius
ω_c = electron cyclotron frequency
$\Delta w_{||}$ = energy gain/loss parallel to the walls after a single "turbulent" or electron-neutral collision.
Γ_1 = total primary electron flux towards a wall
Γ_2 = total flux of secondary electrons emitted from a wall
Γ_i = ion flux to a wall
γ = total secondary electron emission coefficient
γ_{cr} = critical value of the secondary electron emission coefficient for space charge saturated sheath regime
T_{cr} = critical electron temperature for space charge saturated sheath regime with Maxwellian electrons
γ_b = partial emission coefficient of a secondary electron beam
γ_p = partial emission coefficient of plasma electrons
w_b = average energy of a secondary electron beam when it impinges on the wall
w_p = average energy of plasma electrons when they impinge on the wall
Γ_b = primary electron flux towards one wall due to the electrons emitted from the opposite wall
Γ_e = primary electron flux towards one wall due to the collision-ejected electrons from the plasma bulk
α = coefficient of penetration of the beam of secondary electrons through the plasma
$u_{y,z}$ = components of flow velocity of a secondary electron beam in the y and z directions respectively
$T_{ex,z}$ = effective electron temperatures along the x and z axes, respectively
J_z = total electric current density along the z axis
J_{bz} = electric current density along the z axis due to the near-wall conductivity effect

I. Introduction

There is a reliable experimental evidence of the wall material effect on operation of a Hall thruster.[3,4] The existing fluid theories explain this effect due to a strong secondary electron emission (SEE) from the channel walls. The SEE is predicted to weaken insulating properties of the near-wall sheaths and, thereby, (i) to cause cooling of plasma electrons and (ii) to enhance the electron conductivity across the magnetic field. From a practical standpoint, a strong SEE from the channel walls is expected to cause additional inefficiencies due to enhanced power losses in the thruster discharge, and an intensive heating of the channel walls by almost thermal electron fluxes from the plasma. Moreover, because the SEE leads to lower values of the sheath potential drop, ion-induced erosion of the channel walls can be also affected. Although these predictions can be certainly applied for plasmas with electrons, which have a Maxwellian electron velocity distribution function, there is no consensus between the existing fluid[4,5,6] and kinetic models[7,8] on how strong the SEE effects on the thruster plasma are. According to kinetic simulations[1,2,7-9] the electron energy distribution function in a collisionless thruster plasma is depleted at high energy due to electron-wall collisions. Under such conditions, the electron losses to the walls can be hundreds times smaller than the losses predicted by the fluid theories. A similar situation was also reported for other kinds of low-pressure gas discharges.[10,11,12] Note that the deviation of the electron velocity distribution function (EVDF) from Maxwellian does not necessarily mean that the SEE cannot play a significant role in the thruster discharge. In experiments with a Hall thruster operated at high discharge voltages, the maximum electron temperature and the electron cross-field current were strongly affected by the SEE properties of the channel wall materials.[13,14]

In recent particle-in-cell (PIC) simulations, [1,2,9] and in the kinetic study we showed that the SEE effect on power losses in a thruster discharge is quite different from what was predicted by previous fluid and kinetic studies. In simulations, the EVDF is strongly anisotropic, depleted at high energy and maybe even non-monotonic. The electron average kinetic energy in the direction parallel to walls is several times larger than the electron average kinetic energy in direction normal to the walls. Secondary electrons form two beams propagating between the walls of a thruster channel in opposite radial directions, [1,2] (also predicted by Ahedo in the fluid study[15]) In the present paper, we focus on a role of elastic electron scattering (due to electron-atom and Coulomb collisions) in the formation of the EVDF and explain how it influences electron-wall interaction in the thruster discharge. It is shown that for high-performance Hall thrusters, the electron fluxes to the walls are limited by the source of these electrons,

which is determined mainly by the frequencies of elastic electron collisions with atoms and ions. The sheath insulating properties depend on the electron EVDF and, therefore, also on the rate of elastic scattering of plasma electrons. In previous kinetic studies of Hall thrusters, the so-called non-local approach[16] was used for modeling of the thruster plasma. The traditional non-local approach was developed for large gas discharges with overall dimensions of order tens of centimeters, and at pressures above 10mTorr. Under such conditions, the electron mean free path is much smaller than the discharge gap $\lambda_c << H$ and the EVDF is isotropic even for electrons with energy larger than the wall potential. However, the traditional non-local approach can not be applied to collisionless plasmas, $\lambda_c >> H$. For Hall thrusters, because the electron mean free path is much larger than the thruster channel dimensions, the EVDF is predicted to be anisotropic,[1,2] especially for electrons with energy larger than the wall potential. In this work, we show that the anisotropy of the EVDF strongly affects the electron flux to the wall. Practical analytical formulas are derived for wall fluxes, secondary electron fluxes, plasma parameters and conductivity. The calculations based on analytical formulas agree well with the results of numerical simulations.

An important implication of the present work is that future theoretical and experimental studies need to determine the influence of these kinetic effects on the thruster performance, heating and erosion of the channel walls. For instance, a reduction in gas density in the thruster channel might significantly reduce electron fluxes to the walls since the electron-ion collisions are less frequent than elastic electron-atom collisions in xenon plasmas for typical plasma parameters for thruster operation..

II. Electron Velocity Distribution Function in a Channel of Hall Thruster Discharge

Formation of the EVDF in the channel of a Hall thruster discharge was studied using a 1D3V particle-in-cell code. The code, slab geometry and numerical results are described in detail elsewhere. [1,2,,9] Typical results of numerical simulations are shown in Figs. 1 and 2. Here, the discharge parameters are E_z = 52 V/cm, B_x = 91 G, $< v_t >$ = 1.4×10^6 s^{-1}, $v_{turb} = 7.8 \times 10^6$ s^{-1}. The EVDF consists of the bulk electrons and SEE beams.

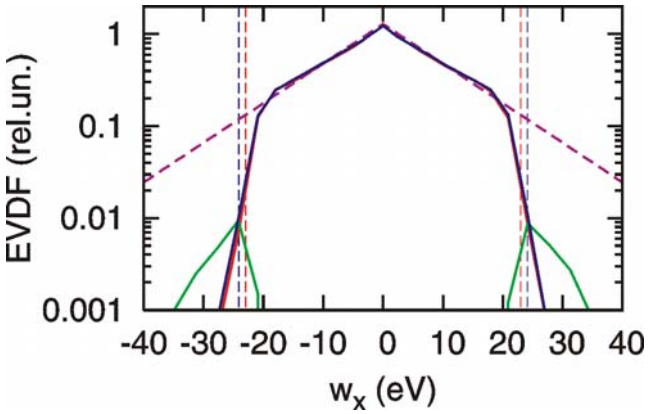

Figure 1 EVDFs over v_x (normal to the walls) in the discharge center plotted versus energy $w_x = m v_x^2/2$ (negative energy values correspond to propagation in the negative direction): bulk electrons in simulation with SEE (solid red curve), SEE beams (solid green curves), bulk electrons in simulation with completely absorbing wall (solid blue curve), and Maxwellian EVDF with T_x = 10.1 eV (dashed magenta curve). Dashed vertical lines indicate the plasma potential in simulation with SEE Φ = 23 V (red)and in simulation with absorbing wall Φ = 24.1 V.

The EVDF is not a Maxwellian. However, in different energy regions the EVDF may be approximated by a Maxwellian EVDF with the corresponding temperature (Figs. 1 and 2). For instance, the EVDF over the normal velocity $f_x(v_x)$ obtained by averaging of the three-dimensional EVDF $f_x(v_x) = \int_{-\infty}^{\infty} dv_y dv_z f(v_x, v_y, v_z)$ is characterized by the effective "normal" temperature T_{ex} (Fig. 1) introduced as the energy value that decreases e times the EVDF over v_x (here e = 2.718…). Similarly, the effective average temperature in the z direction, T_{ez}, may be introduced as the energy value decreasing e times the EVDF over v_z. The exact definitions of these effective

average temperatures are given in Refs. 2 and 9. We found that the ratio between the average temperatures T_{ex} and T_{ez} are better characteristics of the EVDF anisotropy then the ratio of the average energies[1,2,9]. Table 1 summarizes the results of numerical simulation for a number of considered thruster cases. The plasma bulk EVDF is anisotropic, with the temperature in the direction of the applied electric field T_{ez} higher (typically by a factor close to two) than the temperature in the direction normal to the wall T_{ex}.

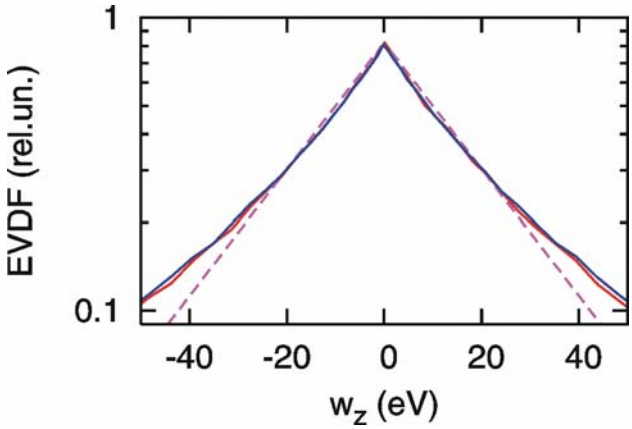

Figure 2 EVDFs over v_z (along the axial E-field) in the discharge center plotted versus energy $w_z=mv_z^2/2$ (negative energy values correspond to propagation in the negative direction): bulk electrons in simulation with SEE (solid red curve), bulk electrons in simulation with completely absorbing wall (solid blue curve), and Maxwellian EVDF with T_z = 20.1 eV (dashed magenta curve).

It is important to emphasize that according to PIC simulations, plasma parameters, including the plasma potential and the electron temperatures are almost insensitive to the SEE. Table 1 summarizes results of self-consistent PIC simulations[1,2,9] for the same thruster input parameters with and without SEE. According to these simulations, the SEE may strongly increase the electron current along the axial electric field. This result will be discussed in the last section of this paper.

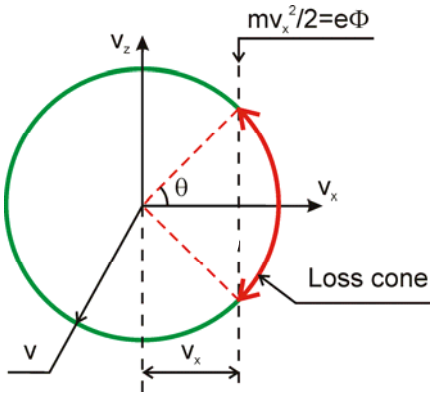

Figure 3 The circle in the two-dimensional velocity space (v_x,v_z) for particles with energy $w = m(v_x^2 + v_z^2)/2 > e\Phi$ or, approximately, $w \approx e\Phi + T_{ez}$. The red section of the circle is the loss cone.

The electrons with the energy sufficient to overcome the sheath potential, quickly escape from the plasma to the wall, where, depending on their energy, they either are lost due to recombination at the wall or produce secondary electrons. In any event, a high energy part of the EVDF is strongly depleted (Fig. 1) and often termed as the loss cone in the phase space.[11,12] The loss cone in two-dimensional velocity space is shown in Fig. 3. Electrons with a given kinetic energy w form a spherical shell in the velocity space. If $w>e\Phi$, where Φ is the plasma potential relative to the wall, then some of these electrons have the energy of motion normal to the wall, w_x, sufficient to leave the system, $w_x > e\Phi$. In the velocity space the vectors of velocities of these electrons are inside the cone with the

opening angle $\theta = 2\cos^{-1}[(e\Phi/w)^{1/2}]$. Note that θ depends on the energy w and $0 < \theta < \pi/2$. The total solid angle in three-dimensional velocity space leading to wall losses to one wall is $\Omega_1 = 2\pi(1-\cos\theta)$, for two walls $\Omega = 2\Omega_1 = 4\pi(1-\cos\theta)$. This cone is called the loss cone.

The loss cone, i.e., the shortage of electrons capable of escaping to the wall ($w_x > \Phi$) in the EVDF is clearly seen in Fig. 1. In the fluid approach, it is implicitly assumed that the loss cone is always filled, which is not the case for most of collisionless plasmas. Therefore, the conventional fluid expressions for the wall electron flux and the sheath potential drop are not so applicable for the thruster plasma. The analytical solution of kinetic equation for the EVDF in the loss cone, f_{lc}, was derived in Ref. 12. The EVDF in the loss cone is replenished due to elastic scattering which transfers electrons from outside of the loss cone to the loss cone, and is emptied due to the free flight to the walls with the rate determined by the transit time ($\sim H/v_x$). In other words, elastic scattering of electrons in the thruster plasma provides a supply of high-energy electrons, which can escape to the channel walls.

Note that for the thruster plasma with $\lambda_c >> H$, the time between collisions λ_c/v far exceeds the transit time H/v. As a result, the EVDF over v_z is not depleted in the high energy tail $w_z > e\Phi$, (Fig. 2). This case is in contrast to collisional low-pressure gas discharges[16] which operate in the limit of $\lambda_c << H$, and where the isotropic EVDF is strongly depleted in the high energy tail, $w > e\Phi$. One could expect that as the gas pressure reduces, the depletion of the EVDF increases due to faster losses of electrons to the walls. However, this intuitive scenario of depletion of isotropic EVDF fails when scattering collisions of electrons are not frequent enough to match the depletion rate of the EVDF in the direction to the wall. Thus, the EVDF in the loss cone is practically empty, but outside of the loss cone it is not depleted due to low loss rate in elastic collisions. For Hall thrusters, the EVDF is depleted in the direction normal to the channel wall, but not in the direction parallel to the wall (Figs. 1 and 2).

The solution of the kinetic equation gives the EVDF as an integral over time of flight of the scattering rate from outside of the loss cone to the loss cone

$$f_{lc}(x,\mathbf{v}) = \int_x^L dx' \frac{1}{v_x} \int_0^{\pi/2} v f(x',\mathbf{v}') \frac{d\sigma}{d\Omega} d\Omega \tag{1}$$

For an isotropic EVDF the integration is straightforward and $f_{lc}(x,\mathbf{v}) = \int_x^L dx' \nu_{en} f(x',v)/v_x$. Therefore, the EVDF in the loss cone is small by a factor of order H/λ_c compared with the EVDF outside loss cone. Here, H is a characteristic size of the plasma bounded between two walls (channel width).

III. Wall Particle Fluxes in Hall thruster Channel

A. The reduced wall electron fluxes due to the depleted loss cone

The electron flux to the wall in the limit of large electron mean free path $\lambda_c >> H$ is given in Ref.12. The wall electron flux is reduced by a factor of order H/λ_c compared with the calculation assuming an isotropic EVDF. For typical thruster conditions $H/\lambda_c \sim 1/100$. For anisotropic EVDF, the integration in Eq. (1) becomes cumbersome. However, for illustration, the electron flux to the wall can be written as

$$\Gamma_e = \frac{H}{8\lambda_c} n_e \sqrt{\frac{8T_{ez}}{\pi m}} \exp\left(-\frac{\Phi}{T_{ez}}\right), \tag{2}$$

Here, n_e is the plasma density in the center, see e.g., Ref. 17. In equation (2) we used the fact that for most of our calculations the temperature in the z-direction is larger than that in the x-direction. Electrons with total energy more than the confinement threshold, $w > e\Phi$, scattered into the loss cone (i.e. lost to the walls) mostly originate from large pitch angle scattering, therefore, the fraction of these electrons and their velocity are determined by the electron temperature in the electric field direction rather than in the direction to the walls. This explains why T_{ez} appears in Eq. 2 instead of T_{ex}.

B. Penetration coefficients of secondary electron emission beams

The secondary electrons emitted from the opposite walls are accelerated in the near-wall sheaths towards the plasma and form counter-streaming beams. For a quasi-stationary symmetric plasma, wall potentials are the same for the opposite walls. When the beam electrons penetrate through the plasma bulk, they may gain enough energy

(due to the E×B motion) to pass the sheath and induce the SEE from the wall. Refs. 1, 2 and 15 introduced a phenomenological penetration coefficient α to describe the loss of the SEE beam current after propagation between the walls. Scattering of the SEE beams can occur due to collisions with atoms or bulk plasma electrons. However, the probability for such scattering to occur is small, (~ few percents) because the electron mean free path is very large for typical thruster collisions. Another scattering mechanism involves high-frequency electric field oscillations with a period shorter or comparable with the time of electron flight through the thruster channel. Such high-frequency electric field oscillations may arise due to the two-stream instability between the SEE beam and the bulk electrons. This instability excites the plasma oscillations with the frequency close to the electron plasma frequency. The necessary condition for this instability is non-monotonic 1D EVDF $f_x(v_x)$. The 1D EVDF can become non-monotonic due to the presence of a very large number of SEE electrons. PIC simulations confirm the predictions of theory. The details of simulations and theory of two-stream instability are given in Refs. 1 and 18.

The two-stream instability results in the energy transfer from SEE beam to bulk electrons, therefore some of SEE beam electrons can not leave plasma because their w_x energy becomes smaller than the wall potential, $w_{x<} \Phi$. This leads to the accumulation of loosely trapped in plasma potential or "weakly-confined" former SEE beam electrons. However, after certain time these electrons can acquire energy from "fresh" SEE beam electrons and leave the plasma. Fig. 4a shows the time evolution of SEE fluxes. About 20 percent of the SEE beam does not reach the opposite wall. However, the reduction of flux is totally compensated by the flux of "weakly-confined" electrons. In PIC codes this reduction may also be attributed to finite number of particles per cell of the computational grid and associated electric field noise.

Summarizing, (i) the effective penetration coefficient should be equal to unity, i.e., all SEE electrons from one wall eventually reach the opposite wall, and (ii) the emitted electron flux is balanced by the sum of fluxes due to the beam and the "weakly-confined" (former secondary) electrons. In other words, the contribution of secondary electrons to the current at the ceramic channel walls is canceled. Therefore, the ion current to the wall is balanced by the flux of bulk electrons scattered into the loss cone. Simulations results presented in Fig.4b confirm this assumption: the ion flux is practically compensated by the collision - ejected electron flux.

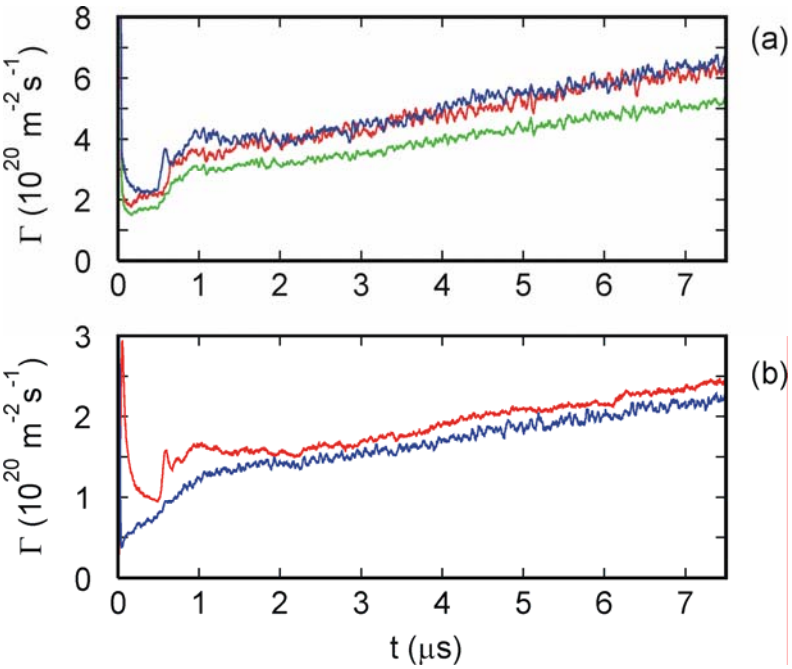

Figure 4 Temporal dependences of wall fluxes obtained in PIC simulation. (a) Secondary electron beam emitted at x=0 (red), secondary electron beam registered at x=H (green), sum of fluxes of the beam and of the weakly-confined electrons at x=H (blue). (b) Ion flux (red) and collision - ejected electron flux (blue) at x=H.

Table 1. Comparison of PIC simulation results with values given by Eqs.(2-4), (10), and (13).

		Simulation number	1	2	3	4	5	6
Simulation parameters (constants) [1, 2,9]		SEE included	Yes	No	Yes	No	Yes	No
		E_z [V/cm]	52	52	200	200	200	200
		B_x [G]	91	91	100	100	100	100
		L [cm]	2.5	2.5	2.5	2.5	3	3
		n_a [10^{12} cm^{-3}]	2	2	1	1	1	1
		ν_{turb} [10^6 s^{-1}]	7.81	7.81	0.7	0.7	0.7	0.7
Values obtained in simulations		Φ [V]	23	24.1	19.4	25.8	24.9	28
		T_{ex} [eV]	10.1	10.6	12.1	11.9	12.1	11.9
		T_{ez} [eV]	20.1	20.4	36.7	41.8	39.3	41.9
		ν_{en} [10^6 s^{-1}]	1.4	1.4	0.7	0.7	0.7	0.7
		λ_c [cm]	1.90	1.91	5.13	5.48	5.31	5.48
		n_e [10^{11} cm^{-3}]	1.93	2.23	1.58	1.70	1.86	1.90
		γ_p	1.18	n/a	1.59	n/a	1.72	n/a
		γ_b	0.564	n/a	0.920	n/a	0.732	n/a
		J_z [A/m^2]	82	89	85	29	45	33
		J_{bz} [A/m^2]	2.3	n/a	58.4	n/a	13.1	n/a
		Γ_i [10^{20} m^{-2} s^{-1}]	2.44	2.76	2.03	2.23	2.65	2.71
Estimated parameters	Eq.(3) with n_e and T_{ex} from simulations	Γ_i [10^{20} m^{-2} s^{-1}]	2.62	3.1	2.35	2.51	2.77	2.80
	Eq.(2) with Φ, and T_{ez} from simulations	Γ_e [10^{20} m^{-2} s^{-1}]	3.04	3.38	2.3	2.31	2.93	2.89
	Eq.(4) with T_{ex} and T_{ez} from simulations	Φ [V]	25.9	25.8	18.6	21.5	27.1	29.2
	Eq.(10) with Φ and T_{ez} from simulations	T_x [eV]	10.7	11.1	12.7	15.6	15.2	16.8
	Eq.(13) with ν_{en}, ν_{turb}, and T_{ex} from simulations	T_z [eV]	27.98	27.69	68.56	68.94	76.85	77.23
	Correction coefficient in Eq. 13 $k \equiv T_{ez}^{(\text{for } k=1)}/T_{ez}^{(\text{PIC})}$	k	1.39	1.36	1.87	1.65	1.96	1.84
	Eq.(18) with γ_p, γ_b, n_e, and T_{ex} from simulations	J_{bz} [A/m^2]	3.2	n/a	68.1	n/a	21.5	n/a

C. Analytical estimate of the wall potential and collision-ejected electron flux

The ion flux can be estimated from the Bohm criterion and the fact that for a planar geometry, the plasma density approximately decreases twice from the plasma center to the plasma sheath boundary in a collisionless case (when ion mean free path is large compared with the channel width), see, for example, Ref. 17:

$$\Gamma_i = \frac{1}{2} n_e \sqrt{T_{ex}/M} \ . \tag{3}$$

The comparison of calculation for electron, Γ_e, and ion, Γ_i, fluxes based on Eqs. (2) and (3) with simulation data shows are shown in Table 1. Agreement between analytical estimate and numerical data is surprisingly good, given the fact that equations are the approximate estimates rather than the exact calculations. The further details of comparison will be given in our future publications.

As explained above, in spite of the presence of a strong SEE, the SEE beams do not contribute to the current balance at the wall. The plasma potential at the center with respect to the wall (i.e. the potential drop in the sheath and pre-sheath) is determined from the ambipolarity criterion that the ion flux is compensated by the collision-ejected electron flux $\Gamma_i = \Gamma_e$. Thus, substituting fluxes from Eqs. (2) and (3) gives

$$\Phi = \frac{T_{ez}}{e} \ln\left(\frac{H}{\lambda_c} \sqrt{\frac{T_{ez}}{T_{ex}}} \sqrt{\frac{M}{2\pi m}} \right). \tag{4}$$

For the conditions in Fig.1, the contribution from the sheath potential gives 5.3, the potential drop in the plasma gives 0.70 and reduction due to empty loss cone gives -5.1 totaling wall potential being of order T_{ez} :

$$\Phi \approx \frac{T_{ez}}{e} \left[\sqrt{\frac{M}{2\pi m}} + \ln 2 - \ln\left(\frac{2\lambda_c}{L} \sqrt{\frac{T_{ex}}{T_{ez}}} \right) \right] = \frac{T_{ez}}{e} (5.3 + 0.7 - 5.1) \approx \frac{T_{ez}}{e} \Phi \ . \tag{5}$$

The first term is the sheath potential; the second is due to the potential drop in the plasma; and the last term accounts for the reduction of the electron flux due loss cone. Note a big contribution of the term describing reduction of the electron flux due loss cone, not described in current fluid and kinetic theories.

Let us emphasis here again that the result of Eq. (5) is only seemingly similar to the result obtained by the fluid theory for the sheath potential drop in the space charge limited sheath regime. The physical meaning of Eq. (5) is fundamentally different because the SEE contribution to the flux balance is self-canceled and, therefore, the plasma potential with respect to the wall does not depend on the SEE.

IV. Reason for Anisotropic Electron Velocity Distribution Function

In a typical gas discharge the EVDF is isotropic i.e., it is a function of the electron speed only f(v). The reason for the isotropic EVDF is that the energy relaxation time for an electron is larger than the scattering time due to collisions or the energy relaxation frequency is smaller than the electron-neutral elastic scattering collision frequency[16]

$$\nu_\varepsilon << \nu_{en} \ . \tag{6}$$

Here, ν_ε is the energy relaxation frequency typically determined by inelastic collisions including excitation and ionization. For electrons with energy larger than the wall potential, wall losses are the fastest energy loss mechanism and the characteristic energy relaxation frequency becomes the frequency of scattering into the loss cone which equals to the electron-neutral elastic scattering collision frequency times the probability of scattering into the loss cone[13] (ratio of the loss cone solid angle, Ω, to the solid angle corresponding to the entire sphere)

$$\nu_\varepsilon \approx \nu_{en}\Omega/4\pi\ . \tag{7}$$

The loss cone into two walls for electron energies at $w = \Phi + T_{ez}$ is

$$\Omega = 4\pi\frac{T_{ez}}{\Phi + T_{ez}}\ . \tag{8}$$

In equation (8) Φ/T_{ez} can be estimated making use of Eq.(4). Under conditions of Hall thruster operation, the wall potential is smaller but comparable with T_{ez} (see Eq.(5) and Table 1) and the loss cone is wide which gives large effective energy relaxation frequency

$$\nu_\varepsilon \sim \nu_{en}\frac{T_{ez}}{\Phi + T_{ez}}\ . \tag{9}$$

As a result, an electron with energy larger than the wall potential does not have time to scatter (isotropize) energy acquired from the electric field in the *z*-direction, and the EVDF is anisotropic. Moreover, because transformation of energy from the *y* and *z*-directions to the *x*-direction occurs due to scatter outside loss cone, $(1-\Omega/4\pi)$, the ratio of temperatures can be estimated as $T_{ex} \sim T_{ez}/(1-\Omega/4\pi)$. Then, using Eq.(8) we obtain

$$T_{ex} \approx \frac{\Phi}{\Phi + T_{ez}}T_{ez}\ , \tag{10}$$

where Φ/T_{ez} can be deduced from Eq.(4). The comparison of Eq. (10) with simulation data is given in Table 1. An agreement between the results of PIC simulations and the analytical estimations is satisfactory, given the fact that these estimations are approximate and performed for the sake of a qualitative analysis.

Note that if the loss cone is small (when $\Phi >> T_{ez}$) then $(1-\Omega/4\pi) \approx 1$ and EVDF becomes isotropic. In the opposite case, when the loss cone is large $\Delta\Omega \to 4\pi$ and $T_{ex}/T_{ez} \to 0$, the anisotropy increases (Table 1).

We shall now derive an expression for the temperature T_{ez}. Figure 2 demonstrates that in the direction of axial electric field, the EVDF can be described as a Gaussian function with a temperature T_{ez}. The flux of energetic electrons to the walls is also determined by this temperature. It is more probable for these energetic electrons to escape to the walls (i.e. to be in the lost cone) than to lose their energy on ionization and excitation (i.e. to be outside the lost cone). Therefore, the electron temperature T_z can be roughly estimated from the balance of electron heating and wall energy losses for these fast electrons. The Joule heating for tail electrons can be written as

$$J_{ezf}E_zH \approx \frac{\nu_{turb}+\nu_{en}}{\omega_c^2 m}e^2E_z^2n_{ef}H\ , \tag{11}$$

where n_{ef} is the effective density of electrons with energy larger than the wall potential, w>eΦ, and J_{ezf} is the current carried by fast electrons. Wall losses can be expressed as $Q \approx \nu_\varepsilon n_{ef}T_{ez}H$, or, substituting ν_ε from Eq. (9),

$$Q_\varepsilon = H\nu_{en}\frac{T_{ez}}{\Phi + T_{ez}}n_{ef}T_{ez}\ . \tag{12}$$

Eqs. (4), (10) –(12) allow to determine the electron temperatures, T_{ez} and T_{ex} and the plasma potential. By equating Eqs. (11) and (12), and using Eq.(4), an approximate expression for the electron temperature in the direction of the electric field is

$$T_{ez} \approx k\left(1+\frac{\nu_{turb}}{\nu_{en}}\right)m_e\left(\frac{E}{B}\right)^2\left(1+\ln\left(\frac{H}{\lambda_c}\sqrt{\frac{T_{ez}}{T_{ex}}}\sqrt{\frac{M}{2\pi m}}\right)\right), \tag{13}$$

where, k is the correction coefficient, which can be obtained by a comparison of the approximate temperature estimations with the *exact* result of PIC simulations. Note that Eq.(13) can be derived making use of energy diffusion coefficient, which is the product of the effective scattering frequency, $(\nu_{en}+\nu_{turb})$, and the energy step, $eE\rho_c$, acquired by an electron from the electric field during spatial step in z-direction on one electron cyclotron radius $\rho_c = v_\perp / \omega_c$.

The comparison of Eq. (13) with simulation data are shown in Table 1. An agreement is again satisfactory given the fact that approximate calculations were performed only as an order of magnitude estimate. The correction coefficient k is varied between 1.4 to about 2. Note that for the thruster conditions in Fig. 1, Eq. 13 can be simplified using Eq. 5: $T_{ez} \approx 2k(1+\nu_{et}/\nu_{en})m_e(E/B)^2$. Also, the correction factor k can be attributed to the fact that the EVDF is not a Maxwellian and Eq.(13) approximates the electron temperature in the EVDF tail only, rather than in the bulk, as given in Table.1.

V. Electron Cross-Field Current Induced by Secondary Electron Emission Beams

Finally, we shall consider the effect of SEE on the electron cross-field current (Table 1). The SEE beams can carry considerable current. The motion of secondary electrons in crossed electric and magnetic fields is given by

$$u_{bz}(x) = -\frac{E_z}{B_x}\sin\left(\omega_c\int_0^x dx\frac{1}{u_{bx}(x)}\right), \tag{14}$$

where $u_{bz}(x)$ and $u_{bx}(x)$ are the beam velocity components. The electric current density along the z direction created by the electrons of a SEE beam and averaged over the channel width is

$$J_{bz} = -\frac{e}{H}\int_0^H dx n_b(x)u_{bz}(x), \tag{15}$$

where

$$n_b(x) = \frac{\Gamma_b}{u_{bx}(x)} = \frac{\gamma_p\Gamma_i}{(1-\gamma_b)u_{bx}(x)} \tag{16}$$

is the beam density, Γ_b and Γ_i are the beam and the ion fluxes towards the wall, γ_b and γ_p are the partial emission coefficients due to the electrons of the beam and the plasma bulk, respectively. Here we used expression for the beam flux from Refs. 1,2 and 9. Assuming for simplicity that the beam velocity normal to the walls is constant, $u_{bx}(x) \approx \overline{u}_{bx} = \sqrt{2e\Phi/m}$, and substituting $u_{bz}(x)$ from Eq.(14) and $n_b(x)$ from Eq.(16) into Eq.(15) with ion flux (3), one obtains

$$J_{bz} \approx \frac{m}{H}\frac{\gamma_p}{1-\gamma_b}\frac{1}{2} n_e \sqrt{\frac{T_{ex}}{M}}\frac{E_z}{B_x^2}\int_0^{\varphi_H} d\varphi \sin\varphi ,. \tag{17}$$

where $\varphi_H = H\omega_c / \overline{u}_{bx}$ is the maximal phase of cyclotron rotation of the beam. PIC simulations with typical Hall thruster parameters show that usually $\varphi_L \approx 2\pi n + 3\pi/2$, where $n = 1,2,\ldots$. Then the integral in (17) is equal to unity, and the electric current density due to the SEE beams emitted from both walls is

$$J_{bz} \approx \frac{m}{H}\frac{\gamma_p}{1-\gamma_b} n_e \sqrt{\frac{T_{ex}}{M}}\frac{E_z}{B_x^2}. \tag{18}$$

This current can significantly contribute to the total conductivity and may explain the influence of wall material on thruster operation observed in experiments[5]. This estimate is similar to Morozov's prediction of the near-wall conductivity[19,20] but we calculated the SEE fluxes self-consistently, from the plasma parameters. Note that the values of γ_p, γ_b depend on the electron temperature, wall potential and electric field.

The physical explanation for the current in Eq.(18) is as follows. The SEE electron during one pass from the wall to the opposite wall moves in the z direction by the distance of order $\rho_c = v_\perp / \omega_c$, where $v_\perp = u_d = E_z / B_x$. Then, the average velocity in z-direction is $\langle u_z \rangle \sim \rho_c / (H / \overline{u}_{bx}) = u_d u_{bx} / H\omega_c$. The expression for the current density $J_{bz} = en_b \langle u_z \rangle$ corresponds to the exact calculation in Eq.(18). Table 1 contains the values of the electric current density due to the SEE beams obtained in simulations and analytically with Eq.(18). There is a reasonably good agreement between the numerical and the analytical values. Note that for simulation 3 in Table 1, the SEE beams create the major part of the current.

VI. Conclusions

We suggested simplified analytical formulas for averaged kinetic plasma parameters of a Hall thruster. Calculations based on derived analytical formulas for the plasma potential, the wall electron flux, and the electron temperatures agree well with particle-in cell simulations results. The SEE effect on power losses in a thruster discharge is shown to be quite different from what was predicted by previous fluid and kinetic studies. The kinetic calculation gives the values of the electron flux of few orders of magnitude smaller than the values obtained in calculation performed making use of the fluid approach. The difference is attributed due to the presence of a large loss cone in the electron velocity distribution function. The EVDF in the loss cone is determined by elastic scattering of electrons due to collisions with atoms and Coulomb collisions.

Another important result of these kinetic studies is that the SEE contribution to the flux balance at the walls is self-canceled and, therefore, the plasma potential with respect to the wall and electron energy losses on the walls are almost insensitive to the SEE. Secondary electrons emitted from the walls form two counter-streaming beams. The effective coefficient for penetration of the SEE beams from one wall to the opposite wall is equal to unity. This is because the electrons, which lose energy and cannot leave plasma in one pass through the channel, will eventually gain energy and escape the plasma. The SEE beams may carry considerable portion of the cross-field electron current due to their cycloid trajectory in ExB field. This may explain the influence of wall material on the thruster operation observed in experiments.[5] The detail analysis of these and other results of these kinetic studies, as well as the generalization of this study for two-dimensional geometry will be discussed in separate papers.

VII. References

[1] Sydorenko, D. Y. and Smolyakov, A. I., "Simulation of Secondary Electron Emission Effects in a Plasma Slab in Crossed Electric and Magnetic Fields" *APS DPP 46th Annual Meeting*, Savannah, GA, November 15-19, 2004, NM2B.008.

[2] Sydorenko, D., Smolyakov, A., Kaganovich, I., and Raitses, Y., "Kinetic simulation of secondary electron emission effects in Hall thrusters" *Phys. Plasmas* **13**, 2006, 014501.

[3] J. Ashkenazy, Y. Raitses and G. Appelbaum, "Parametric studies of the Hall current plasma thruster," *Phys. Plasmas* **5**, 2055 (1998).

[4] Barral, S., Makowski, K., Peradzy´nski, Z., Gaskon, N., and Dudeck, M., "Wall Material Effects in Stationary Plasma Thrusters. II. Near-Wall and In-Wall Conductivity" *Phys. Plasmas* **10**, 2003, pp. 4137, 4152.

[5] E. Ahedo, J. M. Gallardo and M. Martinez-Sanchez, "Effects of the radial plasma-wall interaction on the Hall thruster discharge" *Phys. Plasmas* **10**, 3397 (2003).

[6] M. Keidar, I. Boyd and I. I. Beilis, "Plasma flow and plasma-wall transition in Hall thruster channel" *Phys. Plasmas* **8**, 5315 (2001).

[7] N. Meezan and M. Cappelli, "Kinetic study of wall collisions in a coaxial Hall discharge" *Phys. Rev. E* **66**, 036401 (2002).

[8] O. Batishchev and M. Martinez-Sanchez, Proceedings of the 28th International Electric Propulsion Conference, March 2003, Toulouse, France (Electric Rocket Propulsion Society, Cleveland, OH 2003), IEPC paper 2003-188.

[9] Sydorenko, D., Smolyakov, A., Kaganovich, I., and Raitses, Y., "Modification of Electron Velocity Distribution in Bounded Plasmas by Secondary Electron Emission" to appear in the *IEEE Transactions on Plasma Sciences* (July 2006).

[10] Kaganovich, I., "Modeling of Collisionless and Kinetic Effects in Thruster Plasmas", the IEPC05 paper-096. in Proc. of the 29th International Electric Propulsion Conference, Princeton University, Princeton, NJ, October 31 - November 4 2005, IEPC2005-096.

[11] Tsendin, L.D., "Electron Energy Distribution in Transversly Inhomogeneous Current-Carrying Plasma" *Sov.Phys. JETP* **39**, 1974, pp.805.

[12] Kaganovich, I.D., Mišina, M., Gijbels, R., and Berezhnoi,S.V., "Electron Boltzmann kinetic equation averaged over fast electron bouncing and pitch-angle scattering for fast modeling of electron cyclotron resonance discharge" *Phys. Rev. E* **61**, 2000, pp. 1875, 1889.

[13] Raitses, Y., Staack, D., Smirnov, A., and Fisch N. J., "Space Charge Saturated Sheath Regime and Electron Temperature Saturation in Hall Thrusters" *Phys. Plasmas* **12**, 2005, 073507, 10 p.

[14] Raitses, Y., Staack, D., Smirnov, A., and Fisch N. J., "Measurements of secondary electron emission effects in Hall thruster discharge" *Phys. Plasmas* **13**, 2006, 014502, 4p.

[15] Ahedo, E. and Parra, F. I., "Partial Trapping of Secondary Electron Emission in a Hall Thruster Plasma" *Phys. Plasmas* **12**, 2005, 073503, 7 p.

[16] Kaganovich, I.D. and Tsendin, L.D., "The space- time averaging procedure and modeling of the RF discharge" *IEEE Transactions on plasma science* **20,** 1992, pp.66, 76.

[17] Kaganovich, I.D., "How to Patch Active Plasma and Collisionless Sheath: Practical Guide" *Phys. Plasmas* **9**, 2002, pp.4788, 4803.

[18] Sydorenko, D., Smolyakov, A., Kaganovich, I., and Raitses, Y., *Phys. Plasmas 2006* (to be published).

[19] Morozov, A.I., "Effect of near-wall conductivity in a strongly magnetized plasma" *Zhurnal Prikladnoi Mekhaniki I Technicheskoi Fiziki*, N3, 1968, pp.19.

[20] Kurochkina, V. A., and Shubin, A. P., "Near-Wall Conductivity in Nonuniform Fields" *Sov. J. Plasma Phys.*, **17**, 1991, 806, 3p.